PHYSICAL REVIEW A VOLUME 4, NUMBER 5 NOVEMBER 1971

Absolute Transition Probabilities of Phosphorus*

Myron H. Miller and Randy A. Roig†
Institute for Fluid Dynamics and Applied Mathematics, University of Maryland, College Park, Maryland 20742

and

Roger D. Bengtson
Department of Physics, University of Texas, Austin, Texas 78712
(Received 26 March 1971)

A gas-driven shock tube was used to measure the absolute strengths of 21 P I lines and 126 P II lines (3300 Å < λ < 6900 Å). Accuracy for prominent, isolated neutral and ionic lines is estimated to be 28–40% and 18–30%, respectively. The data and the corresponding theoretical predictions are examined for conformity with the sum rules.

I. INTRODUCTION

Oscillator strengths of the visible phosphorus lines are difficult to determine either experimentally or theoretically. In the visible, prominent neutral and ionic lines originating in thermal light sources tend to blend with one another. Typical excitation potentials are such that interference between the two spectra persists throughout much of the useful [optically thin, local-thermodynamic-equilibrium (LTE)] range of plasma conditions. Furthermore, P I profiles frequently merge together, their Stark (full) half-widths being of order 1.5–4.5 Å at electron densities (5×10^{16} cm^{-3}) which maintain thermal equilibrium. No P I or P II *gf* values have previously been measured[1] at wavelengths longer than 3000 Å. Abundance estimates of phosphorus have relied upon calculated oscillator strengths[2,3] even though it has been recognized that radial wave functions for visible P I lines do not satisfy the usual validity criteria,[4,5] and that the assumptions of *LS* coupling and negligible configuration mixing are probably unjustified for visible P III lines.[5,6]

II. METHOD

A. Selection of Operating Conditions

From the onset of these experiments[7–11] it was realized that the shock tube afforded the opportunity of selectively enhancing the first or second spectra of phosphorus so that P I-P II blending could be minimized. This was done by operating the shock tube within two distinct temperature-pressure regimes. Rankine-Hugoniot equations and empirical analogs of the Taub relations were used as guides for selecting optimal test gas pressures and compositions.[7] The cooler and denser [(8000–9600) °K, and $(0.5–1.5)\times10^{19}$ particles cm^{-3}] set of shocks fully dissociated small concentrations of PH_3 in neon carriers, provided useful P I brightness, and kept P II/P I intensity to a minimum. The relative intensity profile shown in Fig. 1(a) is prototypical of the data recorded under these conditions. Hotter [(11 400–13 000) °K] and less dense [$(0.3–0.5)\times10^{19}$ particles cm^{-3}] plasmas preferentially enhanced the P II spectrum, to an extent that can be judged by comparing parts *a* and *b* of Fig. 1. Sometimes, Stark shifts in opposite directions helped to separate merged lines. Relatively few of the blends involving prominent P I and P II lines could not be unscrambled by comparing data obtained under diverse source conditions.

B. Thermal Balancing

The critical temperature dependence of atomic state populations is often regarded as the principal problem in quantitative emission spectroscopy.[12–16] The Saha-Boltzmann statistics governing the brightness of P I and P II lines are utilized for "thermal balancing," a technique which reduces the temperature dependence implicit in measured A values.[17,18] Figure 2(a) illustrates the thermal dependence implicit in the A values of P I λ5477 measured by different emission techniques. The depicted conditions (test gas = 0.67% PH_3 + 99.33% neon, $p = 1.6\times10^7$ dyn cm^{-2}, and $T = 9000$ °K) are typical of the cooler first-reflected shock plasma. Ordinates show relative error $A(T)/A(T_0)$ in measured A values as functions of the difference between the *measured* temperature T and the *true* temperature T_0. Measurement of the absolute integrated line intensity I_P yields the conventional[17,18] emission result

$$A_P^{em} = (4\pi\lambda/hcl)\, I_P/N_P \,, \tag{1}$$

where N_P is the excited-state number density and l is the thickness of the source. The fixed phosphorus-to-hydrogen ratio of PH_3 and a trans-species measurement of relative intensities I_P/I_H yield the P I λ5477 A value referenced to the H_β A value[17,18]

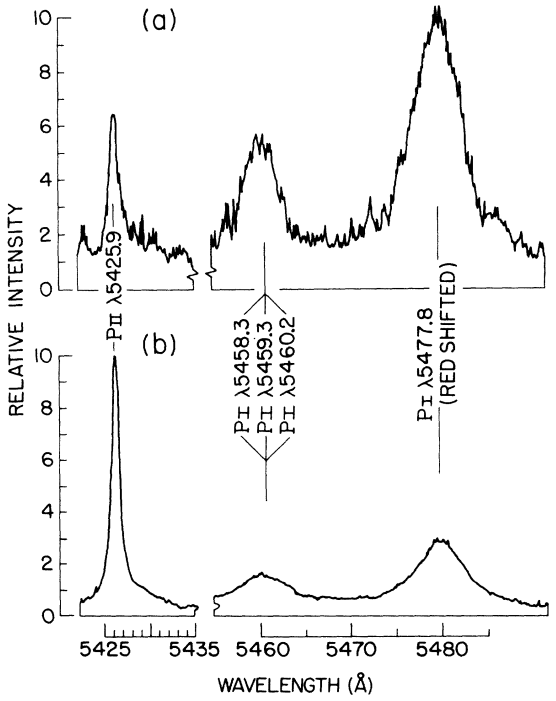

FIG. 1. Samples of the shock tube spectrum of phosphorus. Both spectrograms were obtained with sampling times of 35 μsec and mean resolutions of 0.30 Å. The full wavelength coverage of each exposure is 1700 Å. The brightness of P I relative to P II changes by more than a factor of 6 between the spectra *a* and *b*, which correspond to plasma temperatures of 9200 and 11 300 °K, respectively. The greater absolute brightness of the hotter light source noticeably improves the photographic signal-to-noise ratio.

$$A_P^H = \frac{N_H}{N_P}\,\frac{I_P}{I_H}\,\frac{\lambda}{\lambda_H}\,A_H\,. \qquad (2)$$

When these two independent determinations of the same A value are made simultaneously, their averaged (thermally balanced)[17] result has a lesser net thermal dependence than either A_P^{em} or A_P^H separately.

To differentiate between the various measurements of the P II λ5253 A value, we adopt the following terminology: $A_{P\,II}^{Ne}$ is the result when a trans-species measurement, similar to Eq. (2), is made relative to H_β; $A_{P\,II}^{Ne}$ is analogous to $A_{P\,II}^{H}$, except that (i) Ne I λ5852 serves instead of H_β as the reference A value, and (ii) the phosphrous-to-neon relative abundance is set by initial partial pressures rather than by a stoichimetric ratio. $A_{P\,II}^{em}$ denotes results obtained the traditional way [that is, in the manner of Eq. (1)] using absolute integrated line emission. Relative errors in the above results which would be generated by temperature errors $T - T_0$ are shown in Fig. 2(b). A source of uncertainty not related to temperature is the Ne I λ5852 A value, whose reliability is estimated to be 10%.[19] Consequently, $\frac{1}{2}[A_{P\,II}^{H} + A_{P\,II}^{Ne}]$ is inherently uncertain by at least 5%. Temperature would need to be known to better than ± 0.5%, however, before a traditional $A_{P\,II}^{em}$ determination could approach a similar reliability. It is also of practical importance to note that $\frac{1}{2}[A_{P\,II}^{H} + A_{P\,II}^{Ne}]$ is less sensitive than $A_{P\,II}^{em}$ to possible bias in absolute photometric and pressure data.

Present instrumentation is shown schematically in Fig. 3. Earlier versions,[7-9] which also yielded phosphorus data, had different means of photographic or photoelectric recording, other test section configurations and different shock tube lengths.

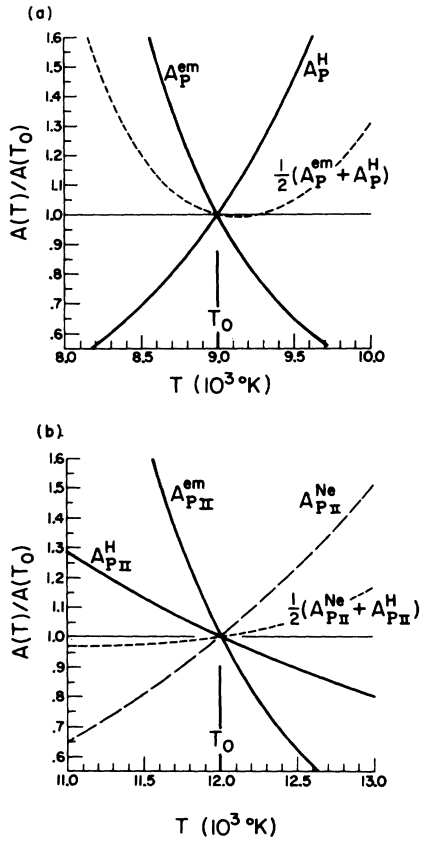

FIG. 2. Sensitivity of experimental A values to hypothetical errors in temperature data. Relative error $A(T)/A(T_0)$ occurs when the assumed temperature T is allowed to vary continuously from the true temperature T_0. (a) Illustration of the behavior of the P I λ5477.7 transition probability measured two ways: in absolute emission (A_P^{em}) and measured relative to H_β(A_P^H). Plasma pressure is 1.6×10^7 dyn cm^{-2}. Initial gas composition is 0.67% PH_3 + 99.33% neon. (b) Corresponding analyses for the P I λ5253.5 A value determined *via* $A_{P\,II}^{H}$ and $A_{P\,II}^{Ne}$. Absolute emission measurements of the conventional type, $A_{P\,II}^{em}$, were not utilized in the present work. The depicted curves are for plasma pressure 1.2×10^7 dyn cm^{-2} and composition 0.14% PH_3 + 99.85% neon.

The optical axes for three polychromators (18 photoelectric channels) and two photographic spectrographs lie in a common plane 2 cm upstream from the tube's reflecting wall. Photoelectric data were used to determine the plasma state and to provide an absolute intensity scale for time-resolved spectrograms.[7,8] Polychromator (e) monitors an optically thick portion of H_α. The continuum flashlamp (h) briefly backlights the shock tube, allowing direct determination of the Planck function. Integrated line and nearby-continuum intensities are recorded by pairs of channels in polychromator (g). A twelve-channel image dissector[7] mounted on the 0.5-m monochromator (f) records intensities in 1.0 Å wide portions of the H_β profile. Spectrographs (d) and (c) have first-order resolutions of 0.24 and 2.3 Å, with useful wavelength coverage of 1700 and 6000 Å, respectively. These two instruments customarily are loaded with pairs of photographic plates having distinctly different response characteristics (γ curves) and spectral sensitivities.[20,21] A fast mechanical shutter (j) is located at an intermediate focal position common to both spectrographs, and provides sampling times of 20–120 μsec.[22] Photomultipliers within (c) and (d) correlate photographic exposure times with diagnostic data recorded by the various polychromators and by the quartz pressure transducers (b) mounted in the shock tube's side and end walls. Spark gaps spaced along the tube trip the delay generators (i), which, in turn, trigger the flashlamp and the fast shutter.

Photomultipliers situated at 6563 Å were calibrated with a regulated carbon arc[12,23] and by a technique utilizing the A value and Stark profile of H_α.[24] Absolute sensitivities determined in these two ways agreed satisfactorily.[24] Photomultipliers recording at other wavelengths were calibrated against the carbon arc anode crater in the customary way.[12,23] Characteristic [density (λ) vs $\log_{10}$ exposure] curves[20,21] were obtained with (i) a seven-step filter, (ii) a continuously variable filter, and (iii) by varying the entrance slit width while photoelectrically monitoring the light incident on the plates. A xenon flashlamp was used to test for reciprocity failure.[20,21] Adjacency effects[20,21] were not detectable for experimentally useful photographic conditions. Consistency between the calibration of the emulsions and the photomultipliers in various polychromators was checked by generating essentially continuous spectra in the shock tube. Shocks in Kr were used for this purpose. Absolute sensitivities were assigned to the photographic exposures in each experiment by fitting data from 8–12 photoelectric channels to appropriate portions of the spectrograms.[7]

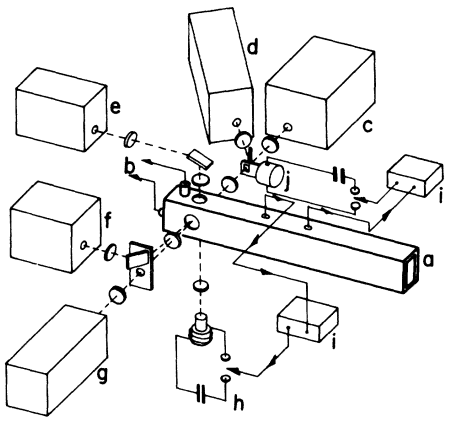

FIG. 3. Diagram of the apparatus: (a) shock tube test section; (b) quartz pressure transducers; (c) medium-resolution spectrograph; (d) high-resolution spectrograph; (e) photoelectric monochromator for reversal measurement; (f) and (g) photoelectric polychromators; (h) reversal flash lamp; (i) delay pulsers for firing flashlamp and shutter, triggered by ionization gauges on shock tube; (j) exploding-wire shutter.

C. Thermodynamic State Determinations

The photoelectrically recorded integrated intensity of Ne I λ5852, with slight optical depth and wing corrections,[16] was combined with pressure data to determine an excitation temperature[3–7] T_{Ne}, for which $E_{up}/kT = 17$–22. A second excitation temperature T_β, with $E_{up}/kT = 12$–15, was obtained from the energy in optically thin H_β. Interaction between optically thick shock tube emission (at 6563 Å) and gray-body flashlamp radiation enabled us to measure the local Planck intensity level.[25] This, in turn, is solved for the radiation ("reversal")[25] temperature, which we denote as T_{rev}. The ionization temperature T_e was calculated by applying modified[26] Saha-Boltzmann equations to pressure and electron density data, the latter being obtained by fitting[27] measured H_β profiles to theoretical Stark shapes.[28]

The various temperatures determined in each experiment are plotted against their average T_{avg} in Fig. 4. Scatter of 3–6% is expected from *a priori* estimates. In perhaps 15% of the experiments, scatter is considerably larger, probably as a result of plasma inhomogeneities. The estimated reliability[9] of T_{avg} for a typical experiment is 2–4%. The agreement between the different types of measured temperatures supports the model we assumed to represent the light source,[7] namely a laminar and homogeneous plasma in local thermodynamic equilibrium.

Plasma pressures measured by the side-wall and end-wall transducers agreed satisfactorily with each other and with pressures calculated from measured shock speeds.[9] Taking into account uncertainties in test gas composition, temperatures, and total

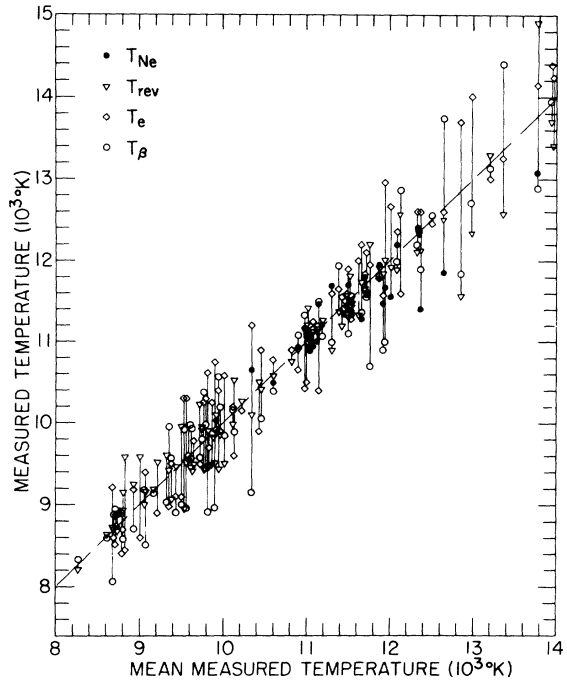

FIG. 4. Comparison of simultaneous and independent temperature determinations with the mean measured temperature per shock.

pressures, it is estimated that the absolute phosphorus abundance in any particular experiment is known to better than 8%.

D. Phosphorus Line Intensities

Profiles of isolated P I and P II lines recorded with 0.24-Å resolution had the expected Voigt shapes, while most of those obtained with 2.3-Å resolution had the truncated appearance of integrated lines.[16] The emulsions used (Kodak I-N, I-F, 103-0, 2475 plates, or in earlier phases of the work, type 103-F and 2475 sheet films)[17] were fast enough for time resolved work, but had two disadvantages: (i) large grain,[20,21] which reduced precision in measuring the area within a typical line profile to 10–20% (per experiment), and (ii) useful (linear) portions of the γ curves generally spanned only $1\frac{1}{2}$ decades in intensity. A single exposure tended to yield optimal data on the brighter or fainter lines in a spectrum, but not both simultaneously.

Spectrograms were read on a digitized densitometer. A computer code[29] converted photographic densities into relative intensities, and incorporated data on temperature and absolute intensity in order to make small optical depth corrections. Laminar shock tube boundary layers form distinctive self-reversal dips in neutral resonance lines, but do not distort ionic lines or those neutral lines whose E_{low}/k exceeds bulk plasma temperature by a factor of 5 or more.[30] On the average, relative line intensities measured by the two spectrographs agreed very well, the deliberate use of different instrumental profiles and emulsion types notwithstanding.

III. RESULTS AND DISCUSSION

More than 50 independent experiments were conducted. Of these 14 were unsuitable for determining absolute A values, either because intensities fluctuated during photographic exposures, film densities were unsuitable, or because scatter in temperature data was anomalously large. Present results for P II are more accurate than for P I, primarily because $\frac{1}{2}[A^{H}_{PII}+A^{Ne}_{PII}]$ is less sensitive to uncertainties in photometric, temperature, or absolute pressure data than is $\frac{1}{2}[A^{em}_{P}+A^{H}_{P}]$.

A. Singly Ionized Phosphorus

Measured absolute P II λ5453 transition probabilities A^{H}_{PII}, A^{Ne}_{PII} and their (shot-by-shot) averages are shown in Fig. 5. Previously estimated random uncertainties adequately account for widths of the various distributions. According to Fig. 2(b), 3% scatter in temperature data imparts a scatter of order 9% to A^{H}_{PII}, 15% to A^{Ne}_{PII}, and 3% to their mean. By compounding this jitter with typical (10–20%) precision for the P II λ5253, H_β, and Ne I λ5852 integrated line profiles, one anticipates scatter (σ) of 32%, 30%, and 20%, respectively, in A^{Ne}_{PII}, A^{H}_{PII} and $\frac{1}{2}[A^{Ne}_{PII}+A^{H}_{PII}]$ results. Bias may arise from the 10% uncertainty in the A value of Ne I λ5852,[19] possible 1–2% bias in T_{avg}, or from unrecognized chemical reaction of PH_3 prior to firing the shock tube.[7] These hypothetical repeatable errors

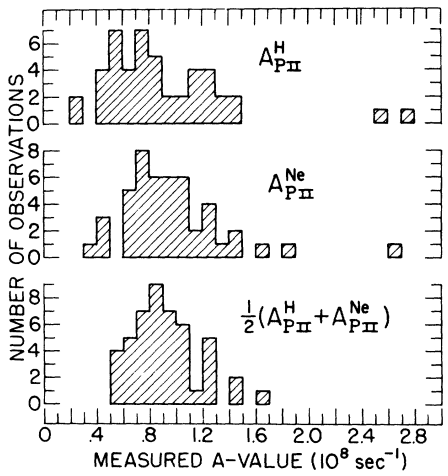

FIG. 5. Histograms of the P II λ5253.5 absolute transition probability measured by three different techniques. Because of thermal balancing, the $\frac{1}{2}[A^{H}_{PII}+A^{Ne}_{PII}]$ data are in principle the most reliable. The adopted result is $(0.92\pm0.17)\times10^8$ sec^{-1}.

would act differently upon A^{H}_{PII} and A^{Ne}_{PII}, and could be responsible for the separation between centers of gravity for these two distributions. *The A value adopted for* P II λ5253 *is* $0.92 \pm 0.17 \times 10^{8}$ sec^{-1}. Our 67% confidence limits are based upon the statistical fluctuations and estimates of possible systematic error.

Present data and comparison material for ionic lines are given in Table I. Blending with P I prevented measurement of two especially prominent lines, P II λ5152.23 and P II λ5483.55. Contrary to expectations based on Martin's observations,[6] we found the ionic lines λ4402.09, λ4414.28, λ4533.96, λ5727.71, and λ5764.64 were too faint to be discriminated from film grain. While λ5225.97 appeared regularly with good brightness, data for this line were not reduced to an A value because of suspected overlapping with an unclassified (P I ?) feature. That is, in variation of brightness with temperature, and in broadening due to Stark effect, the behavior of λ5225.97 was typical of the P I rather than the P II spectrum.

In Table I, the classification by Martin[6] has been used throughout. Martin's relative intensities, divided by upper-state statistical weights, appear in the third column. Although obtained from a nonthermal light source, for visible lines these intensities generally compare more favorably with our relative gA values than do the predictions of LS coupling. In the ultraviolet, however, the relative brightness of weak P II lines in the shock tube disagreed with Martin's intensity scale by as much as a factor of 10. When Martin's data are employed to separate blended pairs of P II lines, the results are regarded as being uncertain by at least 50% even when the merged lines have similar excitation energies.

Transition probabilities recommended in the well-known (NBS) compilation,[5] and listed in the fifth column of Table I (CA-LS), were calculated by assuming LS coupling and Coulomb approximation (CA) radial wave functions. Their typical estimated accuracy is ± 50%.[5] Wherever feasible the authors have made similar calculations[31] to supplement the NBS values. For transitions in the $3d$-$5p$ array, the computed radial wave functions approach cancellation. Strong mixing of $3s3p^3$ with $3s^23p3d$ has been discussed by Martin[6]; lines involving these configurations are not likely to conform well to LS coupling.

One notable feature of Table I is the frequent occurrence, with measurable strength, of LS-forbidden ($\Delta S = \pm 1$, $\Delta L = \pm 2$) lines. Systematic trends[32] in atomic A values have prompted the suggestion[5] that intermediate coupling (IC) would offer a satisfactory description of the P II visible line strengths. A computer code developed by Warner[33] calculates intermediate coupling line strengths with eigenvectors determined from observed energy levels. When applied to the present $3p4s$-$3p4p$ and $3p4p$-$3p4d$ arrays, the code predicted energy eigenvalues differing by more than 1000 cm^{-1} from the observed levels. Therefore, corresponding line strength predictions cannot be regarded as accurate.[34] Presumably, configuration mixing needs to be treated together with IC.

The possibility of undetected experimental bias in our absolute A values can be scrutinized by (i) seeking any functional relationships between the experimental atomic constants and the thermodynamic source conditions used in their measurement, and by (ii) testing our results against the f sum rules.[35,36] To go a step further, the measured relative P II line strengths are examined for the existence of any dependence upon photometric variables. Relative line strengths are also compared with the J file sum rule.[37] While these procedures are not sensitive enough to "verify" claimed accuracies of order 18–22%, they do provide some indirect corroboration for present results, which is felt to be useful in the absence of reliable experimental or theoretical comparison data.

Individual absolute determinations of the P II λ5253 transition probability, normalized to our

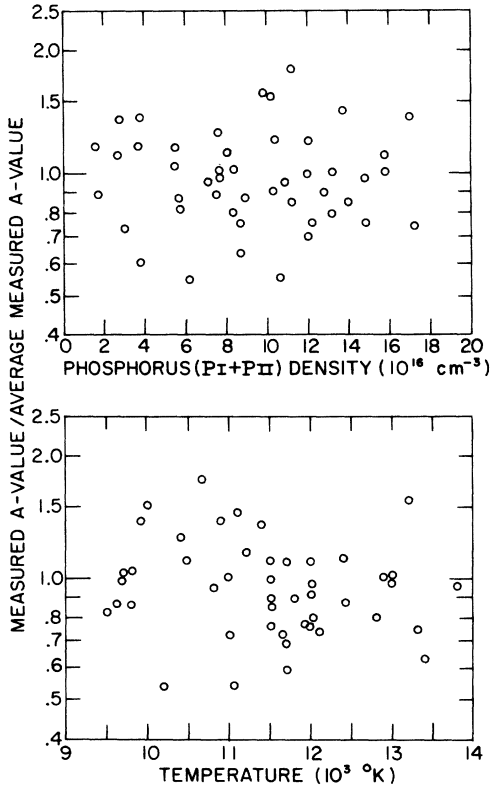

FIG. 6. Measured absolute A values for P II λ5253.5, normalized against the adopted value, show no dependence upon phosphorus densities or upon measured temperatures.

TABLE I. Absolute transition probabilities for P II.

λ(air) (Å)	Combination (Ref. 6)	I_{rel}/g (Ref. 6)	A values (10^8 sec^{-1}) Present work[a]	CA-LS (NBS[2])
3308.92	$3p^3\ ^1D_2^0 - 4p\ ^1D_2$	30.0	0.021 D	...[b]
3318.31	$4p\ ^1P_1 - 4d\ ^1P_1^0$	8.3	0.030 E	...[b]
3377.58	$3p^3\ ^1P_1^0 - 4f\ ^1D_2$	8.0	0.061 E	...[b]
3404.43	$3p^3\ ^1P_1^0 - 4f\ ^3D_2$	10.0	0.073 D	...[b]
3419.34	$3p^3\ ^3P_2^0 - 4p\ ^3S_2$	42.0	0.028 D	...[b]
3424.99	$3p^3\ ^3P_2^0 - 4p\ ^3S_1$	33,0	0.025 E	...[b]
3426.26	$3p^3\ ^3P_0^0 - 4p\ ^3S_1$	17.0	0.011 E	...[b]
3472.98	$3p^3\ ^3P_2^0 - 4p\ ^3p_2$	8.0	0.011 D	...[b]
3475.20	$3d\ ^3D_2^0 - 4f\ ^1D_2$	0.2	0.017 E	...[b]
3478.81	$3p^3\ ^3P_1^0 - 4p\ ^3P_2$	5.0	0.003 D	...[b]
3490.51	$3d\ ^3P_1^0 - 4f\ ^1D_2$	8.0	0.080 E	...[b]
3501.12	$3p^3\ ^1P_1^0 - 5p\ ^1D_2$	2.0	0.006 E	...[b]
3503.07	$3p^3\ ^3P_2^0 - 4p\ ^3P_1$	20.0	0.014 D	...[b]
3507.44	$3d\ ^3D_2^0 - 4f\ ^3D_3$	13.0	0.11 E	0.04
3510.33	$3p^3\ ^3P_0^0 - 4p\ ^3P_1$	2.0	0.002 E	...[b]
3516.25	$3d\ ^3P_0^0 - 4f\ ^3D_1$	8.0	0.12 E	1.2[c]
3518.67	$3p^3\ ^3P_1^0 - 4p\ ^3P_0$	15.0	0.017 E	...[b]
3519.19	$3d\ ^3P_1^0 - 4f\ ^3D_2$	3.0	0.043 D	1.6[c]
3527.19	$3d\ ^3D_1^0 - 4f\ ^1D_2$	3.0	0.025 D	...[d]
3530.32	$3d\ ^3D_1^0 - 4f\ ^3D_1$	10.0	0.11 D	0.30[c]
3533.17	$3d\ ^3P_2^0 - 4f\ ^1D_2$	5.0	0.032 E*	...[d]
3533.68	$3p^3\ ^1D_2^0 - 4p\ ^3S_1$	8.3	0.003 E*	...[b]
3551.26	$3p^3\ ^1P_1^0 - 4f\ ^3F_2$	3.0	0.019 D	...[b]
3556.04	$3d\ ^3D_3^0 - 4f\ ^3D_2$	0.4	0.004 E*	0.06[c]
3556.49	$3d\ ^3D_1^0 - 4f\ ^3D_3$	5.0	0.043 E*	0.06[c]
3559.97	$3d\ ^3D_3^0 - 4f\ ^3D_3$	5.0	0.044 D	0.34[c]
3562.57	$3d\ ^3P_2^0 - 4f\ ^3D_2$	6.0	0.060 D	0.52[c]
3566.51	$3d\ ^3P_2^0 - 4f\ ^3D_3$	5.7	0.054 D	2.1[c]
3570.24	$3d\ ^2D_2^0 - 4f\ ^3G_3$	1.3	0.035 E	...[d]
3617.13	$3d\ ^3D_3^0 - 4f\ ^3G_4$	10.0	0.056 E	...[d]
3623.19	$3p^3\ ^1D_2^0 - 4p\ ^3P_1$	3.0	0.003 E*	...[d]
3624.67	$3d\ ^3D_3^0 - 4f\ ^3G_3$	0.8	0.009 E*	...[d]
3631.46	$3d\ ^3P_2^0 - 4f\ ^3G_3$	3.6	0.034 E	...[d]
3653.49	$3d\ ^2D_2^0 - 4f\ ^3F_3$	3.0	0.118 E	2.4[c]
3659.33	$3d\ ^3D_2^0 - 4f\ ^3F_2$	0.8	0.027 E	...[b]
3664.23	$3d\ ^3D_2^0 - 4f\ ^1F_3$	1.3	0.065 D	...[d]
3676.33	$3d\ ^3P_1^0 - 4f\ ^3F_2$	3.0	0.28 C	...[d]
3706.13	$3d\ ^3D_3^0 - 4f\ ^3F_4$	3.3	0.42 D	2.6[c]
3710.52	$3d\ ^3D_3^0 - 4f\ ^3F_3$	1.1	0.064 E	0.29[c]
3715.90	$3p^3\ ^3P_2^0 - 4p\ ^3D_3$	2.7	0.007 E*	...[d]

TABLE I. (*Continued*)

λ(air) (Å)	Combination (Ref. 6)	I_{rel}/g (Ref. 6)	*A* values (10^8 sec^{-1}) Present work[a]	CA-*LS* (NBS[2])
3717.04	$3d\ ^3D^0_1 - 4f\ ^3F_2$	3.0	0.18 *E*•	2.2[c]
3717.62	$3d\ ^3P^0_2 - 4f\ ^3F_3$	2.2	0.16 *E*•	. . .[d]
3723.67	$3d\ ^3P^0_2 - 4f\ ^3F_2$	1.6	0.092 *D*	. . .[d]
3728.74	$3d\ ^3P^0_2 - 4f\ ^1F_3$	1.1	0.053 *E*	. . .[d]
3761.86	$3p^3\ ^3P^0_2 - 4p\ ^3D_2$	2.0	0.003 *D*	. . .[b]
3768.72	$3p^3\ ^3P^0_1 - 4p\ ^3D_2$	2.4	0.004 *D*	. . .[b]
3793.53	$3p^3\ ^3P^0_1 - 4p\ ^3D_1$	3.3	0.002 *E*	. . .[b]
3795.07	$3p^3\ ^3P^0_0 - 4p\ ^3D_1$	4.0	0.004 *E*	. . .[b]
3827.43	$4p\ ^1P_1 - 4d\ ^1D^0_2$	<2.5	0.44 *E*	0.43[c]
3839.82	$3d\ ^3D^0_2 - 5p\ ^3D_2$	0.4	1.1 *E*	0.002[c]
3851.32	$3p^3\ ^1D^0_2 - 4p\ ^3D_3$	0.4	0.016 *E*	. . .[d]
3857.27	$3d\ ^3P^0_2 - 5p\ ^3D_3$	0.3	0.15 *E*•	0.0002[c]
3858.53	$3d\ ^3P^0_1 - 5p\ ^3D_2$	0.2	0.14 *E*•	0.0001[c]
3885.18	$4p\ ^1P_1 - 4d\ ^3D^0_2$	4.0	0.34 *B*	. . .[d]
3902.86	$3d\ ^3D^0_3 - 5p\ ^3D_2$	0.4	0.020 *E*•	0.0006[c]
3903.39	$3d\ ^3D^0_1 - 5p\ ^3D_2$	0.4	0.020 *E*•	0.0004[c]
3927.34	$3p^3\ ^1D^0_2 - 4p\ ^3D_1$	6.7	0.005 *E*	. . .[d]
4019.53	$3p^3\ ^3P^0_2 - 4p\ ^1P_1$	6.7	0.017 *D*	. . .[d]
4044.61	$3d\ ^1F^0_3 - 4f\ ^1G_4$	5.5	1.37 *A*-	2.4[c]
4062.15	$4p\ ^3D_2 - 4d\ ^3P^0_2$	2.0	0.21 *D*	0.007[c]
4064.73	$4p\ ^3D_2 - 4d\ ^3D^0_1$	2.0	0.26 *D*	0.11[c]
4109.28	$3d\ ^1F^0_3 - 4f\ ^3G_4$	4.4	0.45 *A*-	. . .[d]
4178.48	$3p^3\ ^1D^0_2 - 4p\ ^1P_1$	33.0	0.47 *B*	. . .[d]
4224.52	$3d\ ^1F^0_3 - 4f\ ^3F_4$	3.3	1.3 *C*	. . .[d]
4244.63	$3d\ ^1F^0_3 - 4f\ ^1F_3$	7.0	0.26 *D*	0.30[c]
4288.60	$4p\ ^1P_1 - 4d\ ^3F^0_2$	40.0	0.17 *C*	. . .[d]
4385.35	$4p\ ^1P_1 - 5s\ ^1P^0_1$	67.0	0.91 *A*-	0.40
4417.30	$4p\ ^3P_1 - 4d\ ^3D^0_1$	17.0	0.37 *B*	0.55
4420.71	$4s\ ^1P^0_1 - 4p\ ^1S_0$	400.0	1.1 *A*-	1.6
4424.07	$4p\ ^3P_1 - 4d\ ^3P^0_0$	30.0	0.52 *B*	0.73
4452.46	$4p\ ^3P_1 - 4d\ ^1D^0_2$	20.0	0.43 *A*-	. . .[d]
4463.00	$4p\ ^3P_2 - 4d\ ^3P^0_2$	30.0	0.71 *A*-	0.54
4466.13	$4p\ ^3P_2 - 4d\ ^3D^0_1$	27.0	0.58 *B*	0.04
4467.98	$4p\ ^3P_0 - 4d\ ^3P^0_1$	40.0	0.69 *B*	0.25
4475.26	$4p\ ^3P_2 - 4d\ ^3D^0_3$	29.0	0.95 *A*-	1.3
4483.68	$4p\ ^3P_1 - 4d\ ^3P^0_1$	13.0	0.41 *B*	0.19
4499.24	$4p\ ^1D_2 - 4d\ ^1F^0_3$	29.0	1.12 *A*-	1.4
4530.81	$4p\ ^3P_1 - 4d\ ^3D^0_2$	24.0	0.62 *A*-	1.0

TABLE I. (*Continued*)

λ(air) (Å)	Combination (Ref. 6)	I_{rel}/g (Ref. 6)	*A* values (10^8 sec^{-1}) Present work[a]	CA-*LS* (NBS[2])
4554.83	$4p\ ^3S_1 - 4d\ ^3P_2^0$	24.0	0.65 *B*	0.96
4558.07	$4p\ ^3S_1 - 4d\ ^3D_1^0$	40.0	0.94 *B*	. . .[d]
4565.27	$4p\ ^3S_1 - 4d\ ^3P_0^0$	80.0	1.83 *B*	0.96
4582.17	$4p\ ^3P_2 - 4d\ ^3D_2^0$	5.0	0.26 *C*	0.33
4588.04	$4p\ ^3D_2 - 4d\ ^3F_3^0$	71.0	1.7 *A*	1.7
4589.86	$4p\ ^3D_1 - 4d\ ^3F_2^0$	100.0	2.0 *A*	1.6
4595.51	$4p\ ^3S_1 - 4d\ ^1D_2^0$	6.0	0.41 *B*	. . .[d]
4602.08	$4p\ ^3D_3 - 4d\ ^3F_4^0$	67.0	2.2 *A*+	1.9
4626.70	$4p\ ^3D_2 - 4d\ ^3F_2^0$	60.0	0.39 *D*	0.30
4628.77	$4p\ ^3S_1 - 4d\ ^3P_1^0$	27.0	0.45 *D*	0.88[c]
4658.31	$4p\ ^3D_3 - 4d\ ^3F_3^0$	43.0	0.17 *D*	0.21
4679.01	$4p\ ^3S_1 - 4d\ ^3D_2^0$	16.0	0.24 *C*	. . .[d]
4698.16	$4p\ ^3p_1 - 4d\ ^3F_2^0$	16.0	0.053 *E*[e]	0.01
4700.86	$4p\ ^3D_1 - 5s\ ^1P_1^0$	27.0	0.084 *E*[e]	. . .[d]
4823.68	$4p\ ^3D_1 - 5s\ ^3P_2^0$	12.0	0.19 *E*	0.01
4864.42	$4p\ ^3D_2 - 5s\ ^3P_2^0$	40.0	0.30 *E*[f]	0.11
4927.20	$4p\ ^3D_1 - 5s\ ^3P_1^0$	50.0	0.32 *A*	0.19
4935.62	$4p\ ^1S_0 - 4d\ ^1P_1^0$	23.0	0.84 *C*	0.63
4943.53	$4p\ ^3D_2 - 5s\ ^3P_2^0$	100.0	0.66 *A*	0.63
4954.39	$4p\ ^3D_1 - 5s\ ^3P_0^0$	300.0	1.15 *C*	0.78
4969.71	$4p\ ^3D_2 - 5s\ ^3P_1^0$	100.0	0.70 *A*−	0.58
5191.41	$4s\ ^3P_1^0 - 4p\ ^3S_1$	50.0	0.17 *A*−	0.35
5253.52	$4s\ ^1p_1^0 - 4p\ ^1D_2$	60.0	0.92 *A*+	1.00
5296.13	$4s\ ^3p_2^0 - 4p\ ^3S_1$	133.0	0.88 *A*+	0.55
5316.07	$4s\ ^3p_1^0 - 4p\ ^3p_2$	50.0	0.20 *A*	0.24
5344.75	$4s\ ^3p_0^0 - 4p\ ^3p_1$	100.0	0.41 *A*−	0.32
5378.20	$4p\ ^3p_1 - 5s\ ^3p_2^0$	50.0	0.40 *C*	0.11
5386.88	$4s\ ^3p_1^0 - 4p\ ^3p_1$	100.0	0.51 *A*	0.23
5409.72	$4s\ ^3p_1^0 - 4p\ ^3p_0$	200.0	1.28 *A*+	0.93
5425.91	$4s\ ^3p_2^0 - 4p\ ^3p_2$	80.0	1.07 *A*+	0.69
5437.38	$3d\ ^1D_2^0 - 4f\ ^3F_3$	7.1	0.13 *E*[g]	. . .[d]
5450.74	$4p\ ^3p_2 - 5s\ ^3p_2^0$	80.0	0.40 *E*[g]	0.33
5461.20	$3d\ ^1D_2^0 - 4f\ ^1F_3$	18.0	0.94 *E*[g]	1.65[c]
5499.73	$4s\ ^3p_2^0 - 4p\ ^3p_1$	67.0	0.25 *A*	0.37
5507.19	$4p\ ^3p_1 - 5s\ ^3p_1^0$	67.0	0.55 *B*	0.11
5541.14	$4p\ ^3p_1 - 5s\ ^3p_0^0$	200	1.00 *E*[g]	0.45
5583.27	$4p\ ^3p_2 - 5s\ ^3p_1^0$	67.0	0.89 *E*[e]	0.19
5588.34	$4p\ ^3S_1 - 5s\ ^3p_2^0$	50.0	0.33 *E*[e]	0.15

TABLE I. (*Continued*).

λ(air) (Å)	Combination (Ref. 6)	I_{rel}/g (Ref. 6)	A values (10^8 sec^{-1}) Present work[a]	CA-*LS* (NBS[2])
6024.18	$4s\ ^3p_1^0 - 4p\ ^3D_2$	100	0.56 *B*[f]	0.51
6034.04	$4s\ ^3p_2^0 - 4p\ ^3D_1$	133.0	0.44 *B*[f]	0.37
6043.12	$4s\ ^3p_2^0 - 4p\ ^3D_3$	71.0	0.66 *B*	0.68
6055.50	$4p\ ^1D_2 - 5s\ ^1p_0^0$	83.0	0.070 *E*	0.69
6057.86	$3d\ ^1D_2^0 - 5p\ ^1p_1$	33.0	≤0.4	0.19[c]
6087.82	$4s\ ^3p_1^0 - 4p\ ^3D_1$	117.0	0.29 *A*−	0.27
6165.59	$4s\ ^3p_0^0 - 4p\ ^3D_2$	70.0	0.14 *B*[f]	0.16
6232.29	$4s\ ^3p_2^0 - 4p\ ^3D_1$	33.0	0.034 *E*	0.02
6367.27	$3d\ ^3F_3^0 - 4p\ ^3D_3$	27.0	0.12 *B*	0.02[c]
6435.32	$3d\ ^3F_2^0 - 4p\ ^3D_2$	50.0	0.20 *E*[e]	0.025[c]
6436.31	$4p\ ^1D_2 - 5s\ ^3p_1^0$	43.0	0.15 *E*[e]	. . .[d]
6459.99	$3d\ ^3F_4^0 - 4p\ ^3D_3$	86.0	0.82 *B*	0.21[c]
6503.46	$3d\ ^3F_3^0 - 4p\ ^3D_2$	120.0	1.3 *E*[f]	0.20[c]
6507.97	$3d\ ^3F_2^0 - 4p\ ^3D_1$	200.0	2.2 *E*[f]	0.22[c]

[a]Uncertainty: $18\% \leq A+ \leq 20\%$; $20\% < A \leq 23\%$; $23\% < A- \leq 25\%$; $25\% < B \leq 30\%$; $30\% < C \leq 40\%$; $40\% < D \leq 50\%$; $50\% < E$.

[b]In view of the interaction between $3s3p^3$ and $3s^23p3d$ configurations, transitions involving these configurations have not been calculated.

[c]Author's estimates based on Ref. 31.

[d]Transition forbidden in *LS* coupling.

[e]Blends with a P II line.

[f]Blends with Ne I or with a hydrogen Balmer line.

[g]Blends with a P I line.

adopted result, are plotted in the upper portion of Fig. 6 as functions of measured phosphorus (P I + P II) number density. There is no indication that our experimental A values depend in any regular way upon phosphorus abundance. The lower portion of Fig. 6 discloses no functional dependence of the A values upon measured plasma temperature.

Array averages of absorption oscillator strengths

TABLE II. Transition array average (Average $\equiv \sum_{array} f_{mult} g_{mult} / \sum_{array} g_{mult}$) f values for P II and N II compared with one-electron sum rules.

Spectrum	P II		P II		N II	
Source	Present work		CA-*LS* (Ref. 5)		NBS compilation (Ref. 19)	
Estimated tolerance	Typically 20–40%		Typically 50%		Typically 25%	
Initial states	$3p4p$		$3p4p$		$2p3p$	
Final states	$3pns$	$3pnd$	$3pns$	$3pnd$	$2pns$	$2pnd$
$n=3$	. . .	-0.41_8[a]	. . .	-0.29_0[b]	-0.31_1	0.72_4
$n=4$	-0.42_3	0.93_2	-0.38_8	0.91_1	0.13_2	0.06_8
$n=5$	0.32_4	0.18_3[b]	0.18_8	0.18_3[b]	0.01_5[a]	0.01_6[b]
$n=6-7$	0.03_0[c]	0.08_8[c]	0.03_0[c]	0.08_8[c]	0.00_4[a]	0.00_4[c]
$n=8-\infty$[c]	0.00_6	0.05_7	0.00_6	0.05_7	0.00_2	0.04_6
Continuous[d]	0.01_3	0.20_3	0.01_3	0.20_3	0.00_9	0.19_5
Partial sum	-0.05_0	1.04_5	-0.15_1	1.15_2	-0.15_1	1.05_3
Via WK sum-rule	≈−0.11	≈1.11	≈−0.11	≈1.11	≈−0.11	≈1.11
Sum	0.99[e]		1.00[e]		0.90	
Via TRK sum-rule	≈1.00		≈1.00		≈1.00	

[a]Augmented when necessary by CA-*LS* calculations.

[b]Author's CA-*LS* calculations (Refs. 31 and 32).

[c]Asymptotic expansion $f = \text{const}/(n^*)$ (Refs. 3 and 36).

[d]Hydrogenic approximations (Ref. 36).

[e]Measured f values for $3p4p \rightarrow 3p^3$ transitions are of limited accuracy, but do indicate that this array contributes −0.02 to −0.06 to the f sum.

for all dipole transitions involving the $3s3p$ configuration of P II are listed in Table II. Despite significant differences between our measured values and the CA-*LS* approximations for some of the leading arrays, the sums for both sets of f values show comparable conformity with the Wigner-Kirkwood (WK) and the Thomas-Reichie-Kuhn (TRK) sum rules.[36] Indeed, they conform as well as the corresponding case for the homologous N II ion, where sophisticated calculations provide f values with accuracies of order 25%.[19]

The ratios (measured strength/predicted strength) for observed P II lines are plotted in Fig. 7 as functions of (a) upper state energy, (b) wavelength, and (c) measured absolute strength. These displays would be capable of detecting only a very serious bias, their sensitivity being limited by the ± 50% inaccuracy estimated[5] to be inherent to the calculated (CA-*LS*) line strengths. A nonzero slope in Fig. 7(a) would indicate faulty thermometry, whereas the zero slope of the data reaffirms the finding of Fig. 6, i.e., no correlation between measured A values and plasma temperature. The data in Fig. 7(b) clearly show a trend. However, the lines responsible ($3300 < \lambda < 4000$ Å and $6400 < \lambda < 6600$ Å) for the positive slope are associated with the strongly perturbed $3s^2 3p 3d$ configuration. As mentioned earlier, there are good reasons to question whether single configurations are even 50% reliable for these lines. Aside from this, Figs. 7(b) and 7(c) uncover no problems involving relative photometry or radiative trapping.

The strengths of lines in the $3p4s$-$3p4p$ and the $3p4p$-$3p4d$ transition arrays are suitably ordered in Table III for comparison with the J file sum rule.[37] Strengths that were deduced from Martin's relative brightness data[6] are suffixed M. Except for λ 7845.63, λ 5060.80, and λ 5141.4, these strengths contribute relatively little to the sums. Breakdowns in the proportionality between file sums and file statistical weights $(2J+1)$ might be caused by configuration interactions, variations in radial wave functions (σ^2), or by experimental error. Calculated (CA-*LS*) file sums have been included to indicate that variations in σ^2 are not expected to be negligible within these arrays.

B. Neutral Phosphorus

Strengths of visible P I lines are less well known than those of P II lines in the same spectral region. Experimental uncertainties tend to be larger because the neutrals broaden more and are weaker than the ions, and are consequently more susceptible to error from blending and from photographic noise. Moreover, as has been discussed, the P I transition probability measurements usually have more implicit temperature dependence than do the P II A values. Theoretical treatments must contend with intermediate coupling and configuration interaction,[3-6] as was the case for P II, and with the additional complication of radial matrix elements (σ^2) that are seldom far from cancellation.

Scatter and repeatable error in temperature data might both cause the P I λ 5477.75 measured A value to appear too *large*, as was shown in Fig. 2(b).

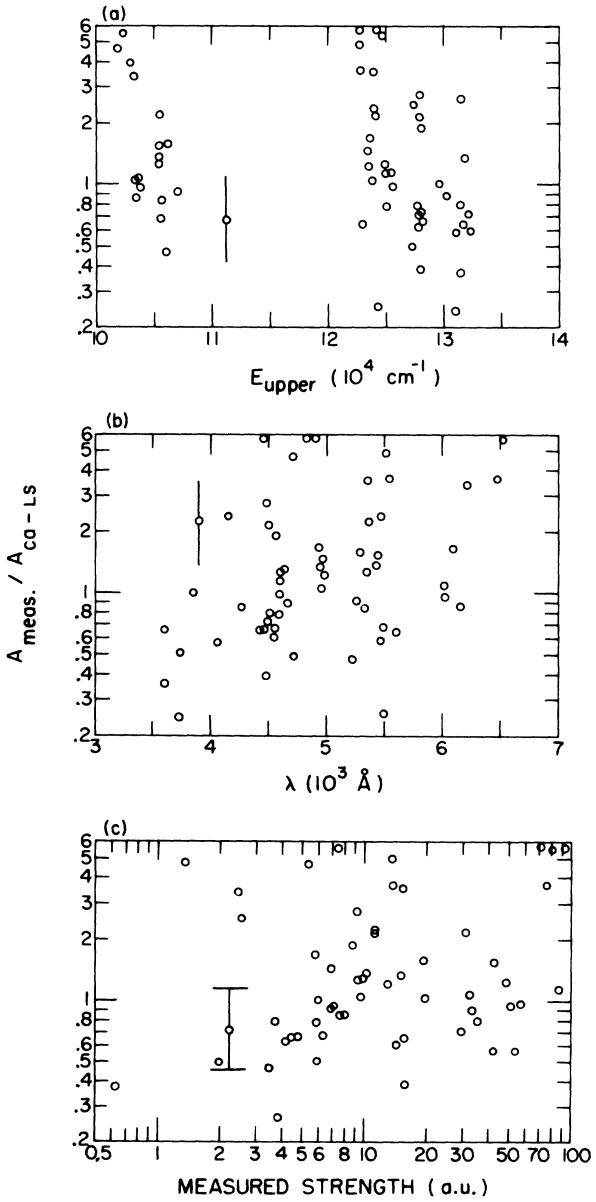

FIG. 7. Tests for bias in the relative P II A values. There are no trends between theory and experiment which depend upon excitation potential or (measured) line strength. The apparent dependence on wavelength is attributed to systematic error in computed A values for lines ($3300 < \lambda < 4000$ Å and $6400 < \lambda < 6600$ Å) belonging to the $3p^3$-$4d$ and $3d$-$4p$ transition arrays.

TABLE III. Line strengths and J-file sums for three P II transition arrays. Line strengths with suffix M were obtained by combining Martin's (Ref. 6) relative intensities and present data for other lines with common upper levels.

$3p4s$ \ $3p4p$	$^1S_0$	$^3P_0$	$^3S_1$	$^1P_1$	$^3P_1$	$^3D_1$	$^3P_2$	$^1D_2$	$^3D_2$	$^3D_3$	$\sum$
$^3P_0^0$			5152.75 1.6M	6647.91 0.4M	5344.75 9.3	6034.12 14.3					25.6
$^1P_1^0$	4420.71 4.6	6121.65 0.1M	5843.61 1.6M	7845.63 23.7M	6092.49 2.4M	7004.61 0.5M	? 0.0	5253.52 32.9	6920.48 0.6M		65.0
$^3P_1^0$	? 0.0	5409.72 10.0	5191.41 3.4	6713.28 2.0	5386.88 11.7	6087.82 9.6	5316.07 7.6	4720.32 0.0M	6024.18 30.2		74.5
$^3P_2^0$			5296.13 19.3	? 0.0	5499.73 6.3	6232.29 1.2	5425.91 42.2	4806.72 0.0M	6165.59 8.0	6043.12 50.4	128.5
$\sum$ NBS (Ref. 5)	6.7	7.2	21.5	23.0	21.7	21.8	36.0	37.0	37.3	52.0	
Present data	4.6	10.1	25.9	26.1	29.7	25.6	49.7	32.9	38.8	50.4	

$3p4d$ \ $3p4p$	$^1S_0$	$^1P_0$	$^3S_1$	$^1P_1$	$^3P_1$	$^3D_1$	$^3P_2$	$^1D_2$	$^3D_2$	$^3D_3$	$\sum$
$^3P_0^0$			4565.27 8.6	? 0.0	4041.89 0.0M						8.6
$^1P_1^0$	4935.62 14.9	? 0.0	? 0.0	3318.31 0.2	? 0.0	? 0.0	? 0.0	4193.47 0.5M	? 0.0		17.8
$^3P_1^0$	? 0.0	4467.98 9.1	4628.77 6.6	3850.48 0.0M	4483.68 5.5	4091.60 1.4M	4533.96 0.5M	? 0.0	4120.82 2.4M		25.5
$^3D_1^0$	? 0.0	4402.09 0.1M	4558.07 13.1	3801.47 0.0M	4417.30 4.7	4036.25 0.2M	4466.13 7.7	? 0.0	4064.73 2.6		28.3
$^3P_2^0$			4554.83 15.2	? 0.0	4414.28 2.8	4033.71 0.2M	4463.00 15.5	? 0.0	4062.15 3.5	4117.16 0.8M	37.2
$^1D_2^0$			4595.51 9.7	3827.43 6.7	4452.46 9.4	? 0.0	? 0.0	5050.80 19.0M	4094.47 0.6	? 0.0	44.8
$^3D_2^0$			4679.01 6.1	3885.18 4.9	4530.81 14.2	4130.81 0.9M	4582.17 3.7	5141.45 8.9M	4160.64 1.2M	? 0.0	60.9
$^3F_2^0$			? 0.0	4288.60 3.2	? 0.0	4589.86 48.2	? 0.0	? 0.0	4626.70 9.5	4698.16 1.4	62.3
$^3D_3^0$							4475.26 30.0	? 0.0	4072.29 0.5M	4127.57 2.2	30.5
$^1F_3^0$							? 0.0	4499.24 35.2	? 0.0	? 0.0	35.2
$^3F_3^0$							5106.03 0.0M	? 0.0	4588.04 56.1	4658.31 5.8	61.9
$^3F_4^0$										4602.08 96.5	96.5
$\sum$ NBS (Ref. 5)	11.0	12.5	36.0	41.0	39.5	46.0	65.0	63.0	78.0	109.0	
Present data	14.9	9.2	59.3	14.4	36.5	50.8	55.4	63.7	76.4	106.7	

TABLE IV. Absolute transition probabilities for P I.

λ(air) (Å)	Combination	I_{rel}/g (Ref. 6)	A values (10^6 sec^{-1}) Present work[a]	NBS (Ref. 5)
5015.86	$4s\ ^4P_{1\,1/2}-5p\ ^4S^0_{1\,1/2}$	1.2	0.087 *C*	2.0
5045.40	$4s\ ^4P_{1\,1/2}-5p\ ^4P^0_{2\,1/2}$	0.8	0.12 *D*	1.6
5061.91	$4s\ ^4P_{1/2}-5p\ ^4P^0_{1\,1/2}$	3.8	0.22 *D*	1.2
5079.37	$4s\ ^4P_{2\,1/2}-5p\ ^4S^0_{1\,1/2}$	13.0	0.51 *B*	2.9
5098.20	$4s\ ^4P_{1\,1/2}-5p\ ^4P^0_{1\,1/2}$	13.0	0.34 *D*[b]	2.9
5100.96	$4s\ ^4P_{1\,1/2}-5p\ ^4P^0_{1\,1/2}$	8.0	0.19 *D*[b]	0.46
5109.62	$4s\ ^4P_{2\,1/2}-5p\ ^4P^0_{2\,1/2}$	7.0	0.27 *B*	3.4
5262.07	$4s\ ^2P_{1/2}-5p\ ^2P^0_{1\,1/2}$	1.0	0.25 *E*	1.5
5293.53	$4s\ ^2P_{1/2}-5p\ ^2P^0_{1/2}$	15.0	0.64 *E*[c]	5.8
5345.86	$4s\ ^2P_{1\,1/2}-5p\ ^2P^0_{1/2}$	18.0	0.65 *C*[c]	7.3
5447.14	$3p^4\ ^4P_{1\,1/2}-4f\ ^4D^0_{1\,1/2}$	7.6	1.2 *E*[c]	•••
5458.31	$4s\ ^2P_{1/2}-5p\ ^2D^0_{1\,1/2}$	25.0	0.83 *D*[c]	3.8
5477.75	$4s\ ^2P_{1\,1/2}-5p\ ^2D^0_{2\,1/2}$	33.0	1.47 *B*	5.7
5514.79	$3p^4\ ^4P_{1\,1/2}-4f\ ^2D^0_{1\,1/2}$	2.5	0.32 *D*[b]	•••
5517.01	$3p^4\ ^4P_{2\,1/2}-4f\ ^4D^0_{3\,1/2}$	12.0	0.32 *D*[b]	•••
5546.92	$3p^4\ ^4P_{1/2}-4f\ ^2D^0_{1\,1/2}$	5.0	0.11 *E*[b]	•••
5548.49	$4s\ ^2P_{1\,1/2}-5p\ ^2D^0_{1\,1/2}$	2.0	0.04 *E*[b]	0.66
5905.02	$4s\ ^2P_{1\,1/2}-5p\ ^2S^0_{1/2}$	25.0	0.36 *E*	•••
6097.68	$4s\ ^2P_{1/2}-4p'\ ^2D^0_{1\,1/2}$	38.0	0.51 *E*[d]	•••
6199.01	$4s\ ^2P_{1\,1/2}-4p'\ ^2D^0_{2\,1/2}$	30.0	0.75 *C*	•••
6210.49	$4s\ ^2P_{1\,1/2}-4p'\ ^2D^0_{1\,1/2}$	10.0	0.13 *C*	•••

[a]Uncertainties: $25\% < B \leqslant 30\%$; $30\% < C \leqslant 40\%$; $40\% < D \leqslant 50\%$; $50\% \leqslant E$.

[b]Blends with other P I lines.

[c]Blends with P II lines.

[d]Blends with Ne I or hydrogen Balmer lines.

However, they cannot cause the experimental A value to err on *small* side. Faulty absolute photometry or an unsuspected loss of phosphorus prior to heating the test gas could cause a decline in A_P^{em} data, but these sources of bias would have practically no effect on the A_P^H data. The satisfactory agreement between A_P^{em} and A_P^H in 39 shock tube experiments persuades us that absolute photometric sensitivities and absolute phosphorus abundances have been correctly assessed.

The absolute A value of P I λ5477.75, determined from $\frac{1}{2}(A_P^{em}+A_P^H)$ measurements, is $1.47 \pm 0.4 \times 10^6$ sec^{-1}, where the uncertainty includes estimates of bias that might arise from blending with P II, P I, or Ne I, or from uncertainties in photometry or thermometry. The predicted A value is 4.3×10^6 sec^{-1}. Theoretical overestimates as large as a factor of 10 are conspicuous features of Table IV.

The CA-*LS* predictions[5] have been regarded as uncertain by "more than 50%." It is not altogether surprising that they are in fact too large by factors of 3–10. Integrals of the radial wave functions approach cancellation. For example, the values of σ^2 in the relatively prominent $4s$-$5p$ array can differ by a factor of 20. Aside from the intermediate coupling that is known[3] to occur, and configuration interactions that are likely to occur, [5] many of the transitions involve core penetrating (s) lower states or equivalent electrons, e.g., $3p^4$. The validity criteria[4] for use of the Coulomb approximation are therefore obviously not satisfied, while the simplifying assumption of *LS* coupling appears to have little justification.

The absolute A values of P I and P II are closely related in these experiments. The ratio of two thermally insensitive results, $[A_P^{em}+A_P^H]/[A_{P\,II}^{Ne}+A_{P\,II}^H]$, itself has very slight implicit dependence on measured temperatures. Typical uncertainties in absolute photometry or in determinations of emitter abundance should transform into relatively minor errors in this ratio. We estimate that the ratio of P I λ5477.75 to P II λ5253.52 A values,

1.47/92, is reliable to 15%. According to the CA and *LS* coupling, this ratio is computed to be 4.3/103.

IV. CONCLUSIONS

Absolute transition probabilities of prominent P I and P II lines ($3300 < \lambda < 6900$ Å) were measured using thermally insensitive techniques. Within a few percent, the better P II data satisfied one-electron f sum rules. The brighter P II lines in the $4s$-$4p$ and $4p$-$4d$ arrays generally had measured strengths that agreed within 40% with the predictions of the CA. Ionic lines originating in the $3s^2 3p 3d$ configuration, however, were factors of 3–10 weaker than estimated theoretically. Presumably, a refined treatment will need to include configuration interactions. Relative strengths of some P II lines were in striking disagreement with the predictions of *LS* coupling, both for the behavior between and within multiplets. Intermediate coupling calculations were attempted, but without provision for configuration mixing these were unable to predict energy eigenvalues consistent with observed levels. Another feature of the data which indicated configuration mixing was that the relative P II line strengths were found not to conform very closely to the J file sum rule. Measured P I transition probabilities were typically factors of 3–10 smaller than had been assumed on the basis of CA-*LS* calculations. No significant portion of this discrepancy can be attributed to experimental error, particularly errors in temperature, since these could only cause measured P I A values to err on the large side. Due to the use of "thermal balancing," the ratio of P I to P II absolute A values for the most accurate data (P I λ5477.75, P I λ5253.52) is estimated to be reliable to 15%.

ACKNOWLEDGMENTS

The authors wish to acknowledge the support and encouragement of T. D. Wilkerson. Suggestions by B. Warner proved to be very helpful. The careful work of B. Latka and J. Clawson facilitated reduction of the data.

---

*Research supported in part by National Aeronautics and Space Administration Grants Nos. NsG-359 and NGR 21-002-007/6. Computer time was provided through NASA Grant No. NsG-398 to the Computer Science Center of the University of Maryland.

†Present address: Physics Department, Harvard College, Cambridge, Mass.

[1]B. M. Miles and W. L. Wiese, Natl. Bur. Std. Spec. Publ. 320 (1970).

[2]A. B. Underhill, Bull. Astron. Inst. Neth. 19, 537 (1968).

[3]Solar abundance of phosphorus is treated by L. Goldberg, E. A. Müller, and L. H. Aller, Astrophys. J. Suppl. 5, 45 (1960); J. W. Swenson, Z. Astrophys. 64, 11 (1966); D. L. Lambert and B. Warner, Monthly Notices Roy. Astron. Soc. 138, 181 (1968).

[4]D. R. Bates and A. Damgaard, Phil. Trans. Roy. Soc. London A242, 101 (1949).

[5]W. L. Wiese, M. W. Smith, and B. M. Miles, *Atomic Transition Probabilities* (U. S. GPO, Washington, D.C., 1969), Vol. II, NSRDS-NBS 4.

[6]W. C. Martin, J. Opt. Soc. Am. 49, 1071 (1959).

[7]M. H. Miller, University of Maryland Report No. RN-550, 1968 (unpublished).

[8]R. D. Bengtson, University of Maryland Report No. BN-559, 1968 (unpublished).

[9]R. D. Bengtson, M. H. Miller, D. W. Koopman, and T. D. Wilkerson, Phys. Fluids 13, 372 (1970).

[10]M. H. Miller, R. A. Roig, and G. A. Moo-Young, Phys. Rev. A 4, 971 (1971).

[11]M. H. Miller, University of Maryland Report No. BN-520, 1967 (unpublished).

[12]J. Richter, in *Plasma Diagnostics*, edited by W. Lochte-Holtgreven (North-Holland, Amsterdam, 1968), Chap. 1.

[13]D. Robinson and P. D. Lenn, Appl. Opt. 6, 983 (1967).

[14]E. W. Foster, Rept. Progr. Phys. 27, 469 (1964).

[15]J. Cooper, Rept. Progr. Phys. 29, 35 (1966).

[16]H. R. Griem, *Plasma Spectroscopy* (McGraw-Hill, New York, 1964).

[17]M. H. Miller, J. Quant. Spectry. Radiative Transfer 9, 1573 (1969).

[18]R. D. Bengtson, M. H. Miller, D. W. Koopman, and T. D. Wilkerson, Phys. Rev. A 3, 16 (1971).

[19]W. L. Wiese, M. W. Smith, and B. M. Glennon, *Atomic Transition Probabilities* (U. S. GPO, Washington, D. C., 1966), Vol. I, NSRDS-NBS 4.

[20]*Kodak Plates and Films for Science and Industry* (Eastman Kodak Company, Rochester, 1963).

[21]C. E. K. Mees, *Theory of the Photographic Process* (MacMillan, New York, 1954).

[22]S. M. Wood and M. H. Miller, Rev. Sci. Instr. 41, 1196 (1970).

[23]A. T. Hattenburg, Appl. Opt. 6, 95 (1967).

[24]M. H. Miller and R. D. Bengtson, J. Quant. Spectry. Radiative Transfer 9, 1573 (1969).

[25]W. R. S. Garton, W. H. Parkinson, and E. M. Reeves, Proc. Phys. Soc. (London) 88, 771 (1966).

[26]H. R. Griem, Phys. Rev. 128, 997 (1962).

[27]R. A. Hill and J. B. Gerardo, Phys. Rev. 162, 45 (1967).

[28]P. Kepple and H. R. Griem, Phys. Rev. 173, 317 (1968).

[29]R. A. Bell, R. D. Bengtson, D. R. Branch, D. M. Gottlieb, and R. Roig, University of Maryland Report No. BN-572, 1968 (unpublished).

[30]M. H. Miller and R. D. Bengtson, Phys. Rev. A 1, 983 (1970).

[31]G. Oertel and L. P. Shono, Astrophys. J. Suppl. 16, 175 (1968).

[32]W. L. Wiese and A. W. Weiss, Phys. Rev. 175, 50 (1968).

[33]B. Warner, Monthly Notices Roy. Astron. Soc. 140, 53 (1968).

[34]J. C. Slater, *Quantum Theory of Atomic Structure* (McGraw-Hill, New York, 1960), Vol. II.

[35]C. W. Allen, *Astrophysical Quantities* (Athlone, London, 1955).

[36]H. A. Bethe and E. E. Salpeter, *Quantum Mechanics of One- and Two-Electron Atoms* (Springer, Berlin, 1957).

[37]E. U. Condon and G. H. Shortley, *The Theory of Atomic Spectra* (Cambridge U. P., Cambridge, England, 1963).

PHYSICAL REVIEW A VOLUME 4, NUMBER 5 NOVEMBER 1971

Calculation of Fine-Structure Splittings and Quadrupole Antishielding Factors for Atomic States*

R. M. Sternheimer and R. F. Peierls

Brookhaven National Laboratory, Upton, New York 11973

(Received 25 June 1971)

As a test of accurate valence wave functions which have been previously obtained for the excited np states of the alkali atoms, we have calculated the fine-structure splittings $\Delta\nu$ using these wave functions. The resulting values of $\Delta\nu_{\text{theor}}$ are generally in good agreement with the corresponding experimental values $\Delta\nu_{\text{expt}}$. Calculations have also been carried out for the atomic quadrupole shielding factor R for the ground states of boron (B $2p$) and aluminum (Al $3p$), and the ionic antishielding factor γ_∞ for the ions B^+, Al^+, and Al^{3+}. The value of $R(\text{B}\,2p) = +0.048$ is in good agreement with the results of calculations using spin-polarization wave functions. The result for $R(\text{Al}\,3p) = -0.063$ leads to a corrected value of the nuclear quadrupole moment $Q(Al^{27}) = 0.140 \pm 0.002$ b, using the atomic-beam result of Lew and Wessel. The ionic antishielding factors γ_∞ have the following calculated values: $\gamma_\infty(B^+) = +0.773$, $\gamma_\infty(Al^+) = -1.68$, and $\gamma_\infty(Al^{3+}) \cong -2.4$.

I. INTRODUCTION

In a recent paper,[1] the present authors have obtained accurate valence wave functions v_{np} for the lowest three excited np states for each of the five alkali atoms. These wave functions were obtained from the requirement that they should be derivable from a potential V_0 which is such that the experimental energy eigenvalues[2] $E_{0,\text{expt}}(np)$ are correctly reproduced. These wave functions were used to obtain accurate values of the quadrupole antishielding factors[3] $R(np)$ for these states. The values of $R(np)$ were used in turn to obtain the corrected values of the nuclear quadrupole moments Q for 12 alkali isotopes. As a check on the wave functions v_{np}, we have calculated (in Ref. 1) the values of $\langle r^{-3}\rangle_{np}$ and also the oscillator strengths $f_{n_0 s - n_0 p}$, where n_0 is the principal quantum number for the lowest excited np state (e.g., $n_0 = 3$ for Na). Both quantities were found to be in good agreement with the corresponding experimental values. (For $\langle r^{-3}\rangle_{np}$, a comparison was possible only for Rb $6p$ and $7p$ and for Cs $7p$ and $8p$.)

It appears that a further test of the wave functions is obtained by calculating the fine-structure splittings $\Delta\nu$ for the alkali atom np states, and by comparing the resulting values with the corresponding experimental values $\Delta\nu_{\text{expt}}$, as obtained from the tables of Moore.[2] This will be done in Sec. II of this paper. It is found that the agreement is very satisfactory (generally within 15%), except for the case of lithium, where the situation has been extensively discussed previously.[4,5]

In previous work, extensive calculations of the quadrupole antishielding factor R have been carried out for the alkali atom np states,[1] and also for the $3d^9\,4s^2$ and $3d^{10}4p$ states of copper,[6] and for the rare earths Pr and Tm (both $5d$ and $4f$),[6] and also for[6] Be $2s2p\,^2P$. For the case of the alkalis and for copper, the valence wave functions were adjusted to reproduce the experimental eigenvalues[2] $E_{0,\text{expt}}$, as discussed above. In addition, Hartree-Fock wave functions were used for the core electrons. It seemed desirable to extend this type of calculations to additional atomic states, and in the present paper, we have carried out calculations for the ground states of aluminum and boron, i.e., for Al $3p$ and B $2p$. The resulting values of R are small, i.e., $|R|$ is less than 0.1 in both cases. The calculations of R for Al $3p$ and B $2p$ are reported in Sec. III.

II. CALCULATIONS OF FINE STRUCTURE

For the fine-structure interval $\Delta\nu$ between the $^2P_{1/2}$ state and the $^2P_{3/2}$ state, the classical formula[7] gives the following result:

$$\Delta\nu = \tfrac{3}{4}\alpha^2 R_\infty \int_0^\infty \frac{1}{r}\frac{dV}{dr} v_{np}^2\, dr\,, \tag{1}$$